Supplemental Materials

Photonic Crystal

The photonic crystal enhances in-band emissivity through the introduction of cavity modes, and is composed of a square array of cylindrical cavities etched into a tantalum substrate. The radius r, period a, and depth d were chosen to match a specific cutoff wavelength. The approximate radius was determined by waveguide cutoff: $r \approx 1.8412 * \lambda_c/(2\pi)$, where λ_c is the cutoff wavelength. The effect of the depth can be intuitively understood from a Q-matching point-of-view: to maximize in-band emissivity, the cavity's absorptive Q and radiative Q should be equal. A higher material absorption (lower absorptive Q) can be matched if r increases and d decreases, as the radiative Q scales as $(d/r)^3$ [1].

The exact dimensions were determined by nonlinear numerical optimization [2] of both finite-difference time domain (FDTD) and rigorous coupled wave analysis (RCWA) simulations [3,4]. The material properties of the substrates were taken into account using a Lorentz-Drude model fitted unstructured tantalum. The geometry was bounded based on fabrication constraints: a minimum space of 100 nm between cavities and the maximum cavity depth was limited to 5.0 µm. The figure of merit used in the optimization was spectral selectivity at a given operating temperature.

Tantalum was used as the substrate for the photonic crystal due to its high melting point, low vapor pressure, advantageous low emissivity in the infrared, and ability to be etched. Sheet tantalum (H. C. Starck) with a thickness of 0.5 mm was cut into 50 mm wafers and polished to mirror finish on one side (Cabot Microelectronics).

The fabrication process, described in Figure 1, begins by deposition of a 100 nm silicon dioxide (SiO_2) etch mask by plasma-enhanced chemical vapor deposition (PECVD), a 250 nm anti-reflection coating (ARC, AZ BARLi) by spin coating, a thin 15 nm protective layer of SiO_2 by electron beam evaporation, and ~200 nm of negative photoresist (PR, THMR-iNPS4, OHKA America) by spin coating. The ARC was necessary to prevent standing-wave induced vertically sinusoidal walls in the PR resulting from reflections from the etch mask. The PR was patterned by interference lithography on a custom built Mach-Zehnder setup with a 325 nm helium cadmium laser [5], to
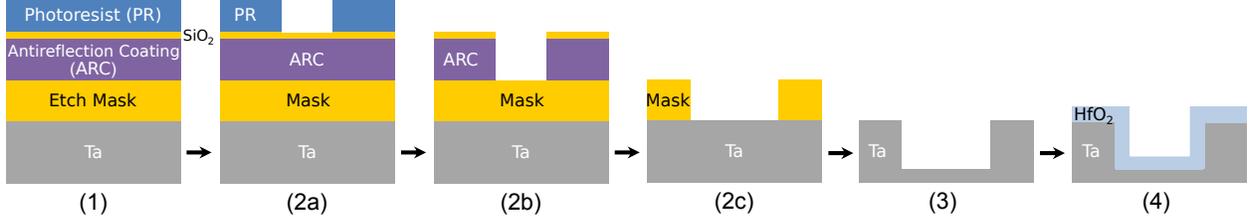
Figure 1: A general process flow for the fabrication of our 2D PhC involves (1) pattern generation, (2) pattern transfer into a hard mask by etching, (3) pattern transfer into the metallic substrate by etching, and (4) conformal coating of PhC with HfO_2 by ALD.

obtain a large periodic pattern with high uniformity. The period was defined by the interference angle, θ, as $a = \lambda/2\sin\theta$. Two orthogonal exposures were used to create a square array of circles, and the cavity diameter was then enlarged to the optimized value by isotropic plasma ashing. The pattern was transfered through the $PR/SiO_2/ARC$ stack by reactive ion etching (RIE, Nexx Cirrus 150), where the SiO_2 serves as a protection layer for the ARC while ashing the PR. The tantalum was etched by deep reactive ion etching (DRIE, Alcatel AMS 100) using a Bosch process using SF_6 and C_4F_8 as the etching and passivating gaseous species. Etching parameters are shown in Table 1. After the final pattern transfer, the residual passivation layer was removed by oxygen plasma and the residual SiO_2 mask was removed by hydrofluoric acid. Finally, a 20 nm conformal layer of HfO_2 was deposited by atomic layer deposition (ALD) at 250°C, using tetrakis dimethylamino hafnium (TDMAH) and water as precursors, to prevent degradation of the surface at high temperatures.

The fabricated photonic crystal was imaged by scanning electron microscopy (SEM) and found to have a period $a \approx 1.3$ µm, radius $r \approx 0.45$ µm, and cavity depth $d \approx 3.0$ µm. The spectral emissivity at room temperature of the photonic crystal was obtained by measuring near-normal incidence reflectance and reflectance at 45° incidence using a Cary 5000 spectrophotometer. Using a least squares method, the geometric parameters were fit to match the measured reflectance, and the best match was for $a = 1.2$ µm, $r = 0.52$ µm, and $d = 5.4$ µm, where the discrepancy in depth may be attributed to both to SEM measurement error because a cross section was not possible and to a higher absorptive Q caused by the scalloped walls or other factors. The same reflectance measurement was also performed after annealing the photonic crystal for 24 hours at 1000°C in a quartz tube furnace in vacuum (5×10^{-6} Torr, heating and cooling rate of 10°C/minute). No

Material	Gases	Flow (sccm)	Pressure (mTorr)	Power (W)
ARC	He/O_2	10/5	7	120
SiO_2	CF_4	15	10	150
Ta	SF_6/C_4F_8	200/100	3	1200/75

Table 1: Parameters used during the RIE processes to etch the tantalum substrate.

change in the reflectance was observed.

Microcombustor

The microcombustor reacts propane and oxygen to heat the photonic crystal to ~1000°C. We used a catalytic design because of the difficulty maintaining a flame at the mesoscale due to thermal and radical quenching at the walls. A planar serpentine channel with catalyst-coated walls provided sufficient interaction time for complete combustion while fitting within external dimensions, which were matched to those of the available PV cells. The channels were dimensioned to provide sufficient length such that the residence time of the gases was much greater than the time for gases to diffuse across the channel, as described in Ref. 6. The microcombustor was suspended by three tubes that doubled as fluidic connections to minimize conductive heat losses. To improve temperature uniformity, a symmetric design was used with two inlets and a central outlet: the increased heat production near the inlet tubes compensated for the increased heat loss due to the edges. In the inlet tubes, propane was delivered via a fine capillary tube run inside the outer tube, and oxygen was delivered via the annulus formed between the capillary and outer tube. This tube-in-tube configuration was necessary to prevent flashback and premature combustion in the inlet tubes.

Inconel 600 (14–17% chromium, 6–10% iron, balance nickel) was used for the microcombustor because of its high-temperature stability in both oxidizing and vacuum environments, low cost, and machinability. More generally, a metallic system was chosen for its compatibility with the tantalum photonic crystal, its robustness to thermal and mechanical shock compared to silicon and ceramics, and its ease of fabrication. The microcombustor was fabricated by diffusion brazing machined components, as shown in Figure 2. Components were fabricated by abrasive water jet cutting from sheet stock. The holes for the tubes were machined to ensure a consistent 25 µm gap

between the tube and hole so that the braze would reliably flow by capillary action. Tubing was commercially available (Microgroup) and was simply cut to length. We bent a loop in the center tube to relieve stress arising from differing thermal expansion between inlet and outlet tubes. Braze preforms were fabricated from foil by photochemical machining using dry film photoresist and ferric chloride etching solution, commonly used for printed circuit board fabrication. Preforms were sized to deliver a slight excess of braze alloy to the joint.

The braze alloy contained melting point depressants, which diffuse into the parent metal during the brazing cycle, allowing the assembly to be reliably operated *above* the brazing temperature. We used BNi-2 (Lucas-Milhaupt) with a solidus temperature of 971°C and a liquidus temperature of 999°C, and the following composition: 7% chromium, 3% boron, 4.5% silicon, 3.0% iron, and balance nickel. The braze alloy was subjected to a prolonged anneal above its liquidus, during which the silicon and boron diffuse out and the molten alloy undergoes isothermal solidification. Assuming the silicon and boron are completely removed, the remelt temperature exceeds 1400°C. The increase in remelt temperature allowed us to use the same braze alloy for all three brazing steps, to avoid exposing the photonic crystal to a higher temperature than absolutely required, and to perform the brazing in a low-cost furnace, which was limited to 1200°C even though the target operating temperature is 1000–1200°C.

Brazing was conducted in three steps: tubes were brazed to the channels, caps were brazed to seal the channels, and the photonic crystals were brazed to the completed microcombustor. Jigs were used to hold components in place for each of the steps. For the first and second brazing operations, the jigs were machined from Inconel. For the final brazing operation, the jig was machined from tantalum to avoid contamination of the photonic crystal, as some outgasing of the Inconel was observed.

Brazing was performed in a quartz tube furnace evacuated by a turbomolecular pump. We relied on the high temperature and high vacuum to shift the chemical equilibrium to favor the dissociation of surface oxides before the braze alloy melted. Flux and reactive atmospheres (e.g. hydrogen) were avoided to prevent contamination of the photonic crystal. After pump-down, the furnace was ramped at 10°C/minute, with one hour stops at 350°C and 500°C for degassing, to a
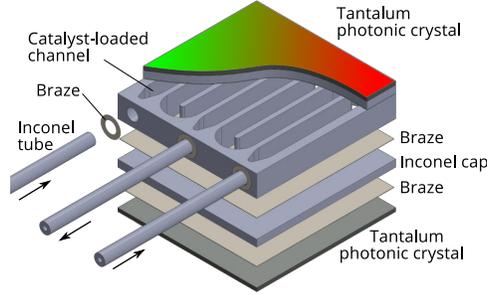
Figure 2: Exploded view of the microcombustor components, which were assembled by diffusion brazing.

final brazing temperature of 1100°C. When the brazing temperature was reached, furnace pressure would initially spike to $\sim 5 \times 10^{-5}$ Torr then reduce to $\sim 3 \times 10^{-6}$ Torr. The temperature was held at 1100°C for two hours to ensure full diffusion before cooling to room temperature.

The finished microcombustor with photonic crystal emitter was brazed into a stainless steel frame for mounting in the experimental apparatus with a gold-nickel eutectic alloy (Lucas-Milhaupt).

The final fabrication step was application of the catalyst, applied as a washcoat. We used a 10 wt% suspension of 5 wt% platinum on porous alumina (Sigma Aldrich 311324) in a 2 wt% solution of nitrocellulose in an organic solvent. We filled the microcombustor though the tubes then blew it out with compressed air, leaving a thin coating on the walls. Upon initial heating, the nitrocellulose decomposed without residue.

References

[1] M. Ghebrebrhan, *et al.*, *Physical Review A - Atomic, Molecular, and Optical Physics* **83**, 1 (2011).

[2] S. G. Johnson, The NLopt nonlinear-optimization package.

[3] A. F. Oskooi, *et al.*, *Computer Physics Communications* **181**, 687 (2010).

[4] V. Liu, S. Fan, *Computer Physics Communications* **183**, 2233 (2012).

[5] M. E. Walsh, On the design of lithographic interferometers and their application, Ph.D. thesis, Massachusetts Institute of Technology (2004).

[6] W. R. Chan, *et al.*, *Journal of Physics: Conference Series* (2013), vol. 476, p. 12017.